We are IntechOpen, the world's leading publisher of Open Access books Built by scientists, for scientists

4,800
Open access books available

122,000
International authors and editors

135M
Downloads

Our authors are among the

154
Countries delivered to

TOP 1%
most cited scientists

12.2%
Contributors from top 500 universities

CLARIVATE ANALYTICS BOOK CITATION INDEX INDEXED

WEB OF SCIENCE™

Selection of our books indexed in the Book Citation Index in Web of Science™ Core Collection (BKCI)

Interested in publishing with us?
Contact book.department@intechopen.com

Numbers displayed above are based on latest data collected.
For more information visit www.intechopen.com

Chapter

Synthesis and ESR Study of Transition from Ferromagnetism to Superparamagnetism In $La_{0.8}Sr_{0.2}MnO_3$ Nanomanganite

Mondher Yahya, Faouzi Hosni and Ahmed Hichem Hamzaoui

Abstract

Electron spin resonance (ESR) spectroscopy was used to determine the magnetic state transitions of nanocrystalline $La_{0.8}Sr_{0.2}MnO_3$ at room temperature, as a function of crystallite size. Ferromagnetic nanoparticles having an average crystallite size ranging from 9 to 57 nm are prepared by adopting the autocombustion method with two-step synthesis process. Significant changes of the ESR spectra parameters, such as the line shape, resonance field (Hr), g-factor, linewidth (ΔHpp), and the low-field microwave absorption (LFMA) signal, are indicative of the change in magnetic domain structures from superparamagnetism to single-domain and multi-domain ferromagnetism by increase in the crystallite size. Samples with crystallite sizes less than 24.5 nm are in a superparamagnetic state. Between 24.5 and 32 nm, they are formed by a single-domain ferromagnetic. The multi-domain state arises for higher sizes. In superparamagnetic region, the value of g-factor is practically constant suggesting that the magnetic core size is invariant with decreasing crystallite size. This contradictory observation with the core-shell model was explained by the phenomenon of phase separation that leads to the formation of a new magnetic state that we called multicore superparamagnetic state.

Keywords: magnetic nanoparticles, perovskite manganite, ESR, ferromagnetism, superparamagnetism, multicore superparamagnetic, phase separation

1. Introduction

Magnetic nanoparticles (MNPs) display physical and chemical properties different those found in their corresponding bulk materials. These properties make them attractive in widespread applications such as energy, electronics, sensor designs of all kinds, catalysts, magnetic refrigeration, optics, and in various biomedical applications [1–6].

In medicine, MNPs has attracted attention because they are detectable, remotely manipulable, stimulable by a magnetic field, and can combine both diagnosis and therapy in one dose. These multifunctional nanomaterials can be used as contrast agents for medical imaging and nano-vectors to transport therapeutic agents to their target, in local delivery of drugs, or to destroy the cancer cells by local hyperthermia [7–10]. These magnetic platforms should possess very small size and must combine high magnetic susceptibility and loss of magnetization after removal of the magnetic field [11, 12]. The optimization of the

nanoparticles' size, size distribution, agglomeration, coating, and shapes along understanding the changes in magnetic properties prompted the application of magnetic nanoparticles in diverse fields.

The magnetic properties arise from the magnetic moment associated with electron spin. In ferromagnetic materials, groups of atoms band together into areas called domains, in which all the electrons have the same magnetic orientation. Fundamental changes occur in ferromagnetic materials when their physical size is reduced. The magnetic structure of the ferromagnetic material consists of several magnetic domains and thus retains an important magnetic moment in zero fields [13]. When the particle size becomes smaller, there is a limit when it becomes energetically unfavorable with the formation of several domains and the particle becomes magnetic single domain. A single-domain particle presents all the spins aligned in the same direction. The critical size value depends on the material. A single-domain particle presents all the spins aligned in the same direction. The total magnetic moment of the nanoparticles can be regarded as one giant magnetic moment, composed of all the individual magnetic moments of the atoms. These nanoparticles show a certain preference for the direction, along which their magnetization aligns to (directions of easy magnetization). As particle size continues to decrease below a critical size, the ferromagnetic material is transformed into a superparamagnetic one. In this case, magnetization can randomly flip direction under the influence of temperature, causing the residual magnetization to be null (**Figure 1**) [14]. Superparamagnetic nanoparticles are preferred in biomedical applications because they have zero magnetization at room temperature and do not agglomerate [15, 16].

Magnetic measurements such as vibrating sample magnetometry and associated methods for determining magnetization according to the applied field and Mössbauer spectroscopy have been extensively used to observe the superparamagnetic behavior [17–19]. In this study, electron spin resonance (ESR) spectroscopy was used to study magnetic properties of $La_{0.8}Sr_{0.2}MnO_3$ nanopowders. The basic concepts of ESR are based on the Zeeman effect which leads to the separation of the energy levels of the electrons under the effect of an external magnetic field. The magnetic moments of the electrons perform a precessional motion around the direction of the applied magnetic field with the angular velocity of Larmor. Classically, the resonance event occurs when a transverse alternating field is applied at the Larmor frequency. For a ferromagnetic solid, a strong coupling exists between the electrons. In general, this energy is more

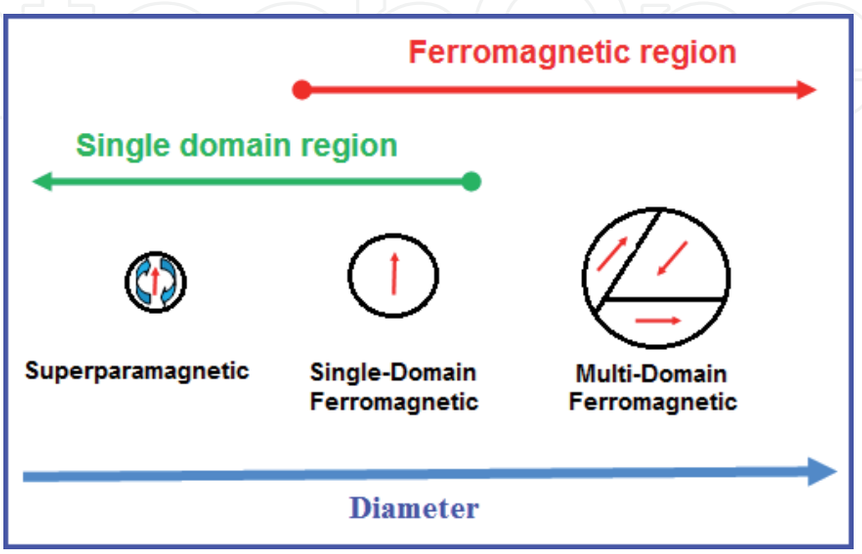

Figure 1.
Transition from multidomain to single-domain to superparamagnetic state whith increasing the particle diameter.

important than Zeeman energy. Thus, in the presence of an applied field, it is the total magnetization which will presage a precession movement [20].

ESR spectra is formed by two absorption, one to the higher fields known as the electronic magnetic resonance (EMR) and an absorption around zero magnetic field appointed low-field microwave absorption (LFMA) [21]. EMR spectrum is a resonant absorption characterized by means of two parameters, the resonant magnetic field (Hres) and the linewidth (ΔHpp). These parameters give information on magnetic nature of the materials [22]. LFMA signal is a nonresonant absorption considered as a sensitive detector of magnetic ordering [23, 24]. This signal has been used to detect the magnetic states in materials and provide highly sensitive detection of magnetic order [23]. More importantly, this signal is not present in the paramagnetic state and emerges as the temperature is lower than Curie temperature [25, 26].

Magnetic homesteads of $La_{1-x}Sr_xMnO3$ perovskites are influenced by intrinsic properties (composition and structure) and extrinsic properties (particle and crystallite sizes depending on the synthesis procedure). Their Curie temperature strongly depends on the Sr-content, and it varies between 320 and 370 K for $0.2 \leq x \leq 0.3$, which makes them attractive for self-controlled magnetic hyperthermia applications. Thus, by applying a high-frequency magnetic field, the magnetic nanoparticles reach their own heating temperature, which does not exceed TC [6, 27]. Their magnetization is higher than that of most materials for such applications [28].

Magnetic phase transitions as a function of temperature and crystallite size have been extensively studied in the past [29–31]. But there are controversial studies in critical sizes of the ferromagnetic- single magnetic domain-superparamagnetic transitions. The critical size is given as a function of the particle size determined by transmission electron microscopy (TEM) or by the crystallite size from DRX data calculated by the Scherrer method. For manganite particles, single magnetic domain is observed in the literature less than diameters which range between 50 and 80 nm [32–34]. Based on crystallites, the change from a multi-domain state to a single-domain state is given in the literature for sizes varying between 26 and 36 nm [34, 35], and crystallite size of the superparamagnetic transition is estimated at 11 nm [28], and between 18 and 24 nm [33, 34, 36].

The observed disparity between crystallite size and particle size is attributed to the polycrystalline nature of the particles. In this work, we will refer to the samples with their corresponding crystallite size.

For this reason, in order to determine critical sizes, we discuss crystallite size dependence of the transition from ferromagnetism to superparamagnetism at room temperature of $La_{0.8}Sr_{0.2}MnO_3$ nanoparticles by using electron spin resonance technique. These transitions are quantified by means of Hres, ΔHpp, and LFMA. To our knowledge, studies on nanoparticles of manganite with LFMA signal are scarce. Therefore, in this work, LFMA signal is used to give knowledge on magnetic state. For this purpose, to obtain the $La_{0.8}Sr_{0.2}MnO_3$ (LSrT-t) nanoparticles with different crystallite sizes, the autocombustion method was adopted with a two-step synthesis process. This method permits to prepare powders in a wide range of crystallite sizes depending on the annealing temperature (T) and heat treatment time (t).

2. Experimental methods

2.1 Autocombustion synthesis

After several years of intense research efforts, it has emerged that a large number of synthesis approaches to a wide variety of nanoparticles are available. In this work, $La_{0.8}Sr_{0.2}MnO_3$ (LSr) nanocrystalline were synthesized by the autocombustion process

with two-step synthesis process. It is an interesting synthetic route for the preparation of a compound with differing crystallite sizes. The reaction is very simple and involves just lanthanum nitrate, strontium nitrate, and manganese acetate. Manganese acetate was dissolved in the minimum of distilled water under agitation. On the other hand, stoichiometric amounts of lanthanum nitrate and strontium nitrate are dissolved in distilled water under stirring. The solution was prepared by mixing aqueous solutions of ($La(NO_3)_3$ + $Sr(NO_3)_2$) and manganese acetate in 1:1 molar ratio. To evaporate the water, the solution was stirred in a beaker placed on a hot plate at 80°C until a viscous product was obtained. The solutions are mixed and were kept stirred in a beaker on a hot plate at 80°C to evaporate the water until you get a product with viscous appearance. After that, the gel obtained was inserted into a preheated oven at 350°C for 2 h. After a few seconds, a violent flame was produced by releasing large amounts of gas, with formation of a spongy powder of dark brown color. Finally, the powder resulting from autocombustion was calcined at 700°C under different heat treatment times and at 800, 900, and 1000°C for 15 h. The samples are designated by LSrT-t (T, calcination temperature; t, heat treatment times).

Phase analysis of all products was performed by using powder X-ray diffraction (XRD) using an X'Pert Pro PANAnalytical diffractometer with CuKα radiation (λ = 1.5418 Å) at room temperature. The crystalline phases were determined by comparison of the registered patterns with the International Center for Diffraction Data (ICDD) powder diffraction files (PDF).

The average crystallite sizes of the samples were estimated from the (0 2 4) reflections at 2θ = 46°, by means of the Debye–Scherrer equation: $D = K\lambda/\beta \cos\theta$, where K is a constant equal to 0.89, λ is the wavelength of the X-ray used, and β is the full width at half maxima (FWHM) of the X-ray reflection at 2θ [37]. The reflection at 2θ = 46° was selected to calculate the crystallite sizes because it does not overlap with other profiles [38, 39].

Magnetization at various fields was measured at temperature 300 K using a vibrating sample magnetometer (VSM) in fields up to 5 T.

We have recorded the ESR spectra of $La_{0.8}Sr_{0.2}MnO_3$ at room temperature, with a Bruker ER-200D spectrometer, operating in the X-Band (9.30 GHz). These measurements are performed on 20 mg of loosely packed fine powder. Data were acquired with 2 mW of power, with a spectral width of 0–8000 Gauss. The ESR signal measured presents the first derivative of the microwave absorption over the magnetic field. The different magnetic state transitions are quantified by means of Landé factor (g), linewidth (ΔHpp), resonant field Hres as function of crystallite sizes, and low-field microwave absorption. The maxima and minima in the derivative signal define the peak-to-peak distance (ΔHpp); the Landé g-factor (g) is calculated based on the equation $g = h\nu/\mu BHres$ where h is Planck's constant, ν is microwave frequency, μB is Bohr magneton, and Hres defines the resonance field determined by the zero-crossing point (dp/dH = 0) [40].

2.2 Structural properties

Figure 2(a) shows the XRD patterns of the precursor and the powders calcined at 700°C (LSr700- t). It seems that all patterns share the same characteristic peaks, indicating that the manganite with perovskite structure has been formed for all samples. Their widths confirm that the $La_{0.8}Sr_{0.2}MnO_3$ powders obtained were in the form of nanocrystals. For precursor powder (sample without any extra heat treatment LSrp), the characteristic peaks of perovskite phase appear with small extra peaks at θ = 25.6, 30 and 39° related to La2O3 phase (JCPDS 83-1355); hence we did not include it in our studies. The high heat released during autocombustion leads to forming the perovskite phase with small amounts of impurities. Calcination

at 700°C during 0.5 h is sufficient to obtain the pure phase. This shows that precursor powder obtained from the autocombustion is very reactive. All peak positions were indexed with perovskite-type crystalline structure of $La_{0.8}Sr_{0.2}MnO_3$ (JCPDS 53–0058) with a rhombohedral space group R-3c. By increasing the heat treatment times, the width of the diffraction peaks decreased, suggesting an increase in the crystallite size. The evolution curve of the average sizes given by the Scherrer formula as a function of the heat treatment times is of sigmoid shape (**Figure 2(b)**). The sizes rapidly increase with treatment durations less than 5 h, to reach an

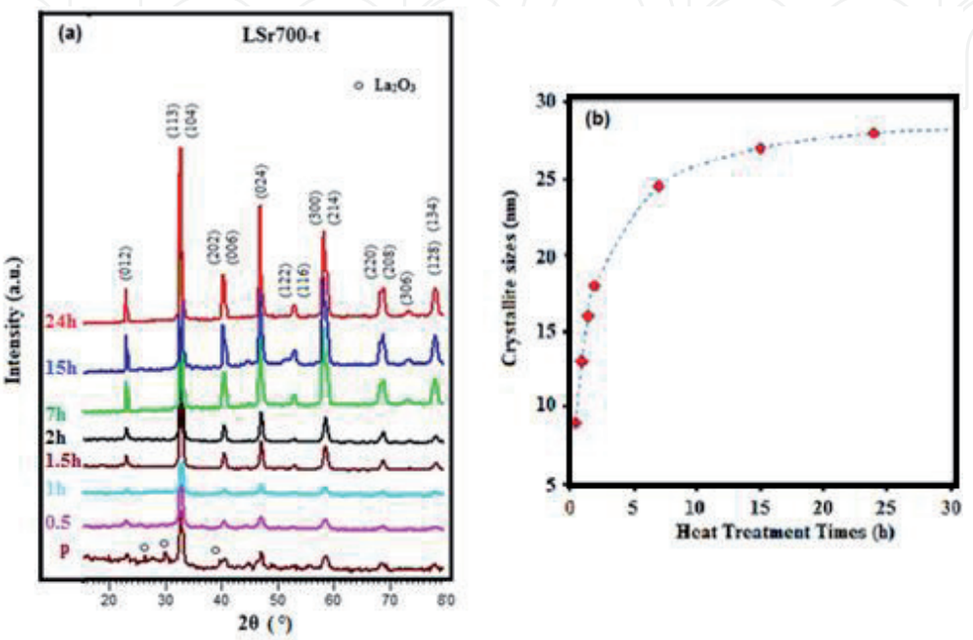

Figure 2.
(a) X-ray diffraction patterns of the samples prepared at 700°C for different processing times. (b) Variation of crystallite size with heat treatment time [20].

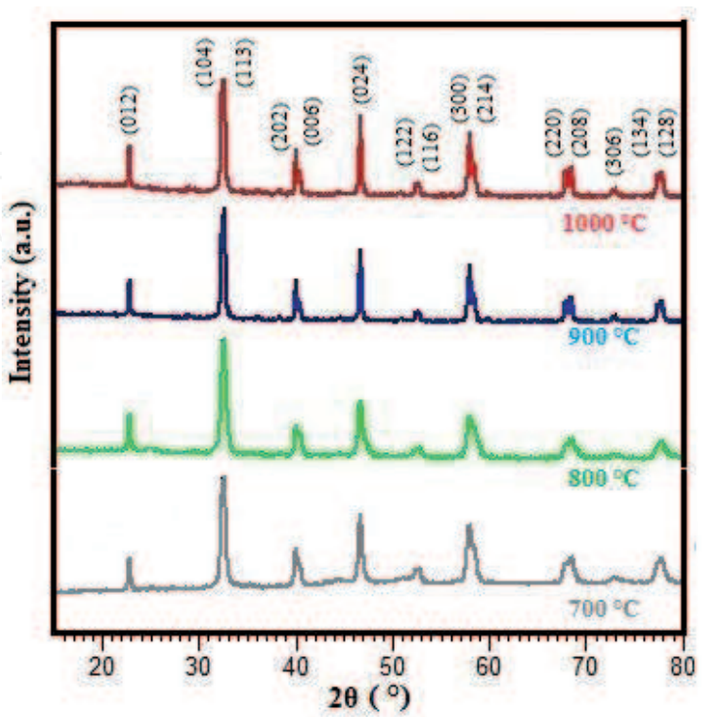

Figure 3.
X-ray diffraction patterns of samples calcined for 15 h at 700, 800, 900 and 1000°C.

asymptote at 28 nm for times greater than 15 h. By increasing the calcination temperature to 800, 900, and 1000°C for 15 h, the widths of the peaks gradually decreased (**Figure 3**). Their crystallite sizes are equal to 32, 55, and 57 nm, respectively.

The autocombustion method offers the advantage of being an exothermic process, self-propagated, and initiated at low temperature. The exothermic reaction between acetate and nitrate ions leads to the formation of the perovskite phase. The nucleation by rearrangement of short-range networks of neighboring atoms is favored by heat treatment. Modified heat treatment conditions such as the temperature and the duration of the heat treatment allowed to prepare a nanocrystalline powder of sizes between 9 and 57 nm [20].

3. Magnetic studies

The ESR spectra obtained from room temperature of all LSrT-t samples are shown together in **Figure 4**. In the first observation, the absorption signal changes radically with crystallite sizes. Two limiting cases are distinguished. For the sizes smaller than

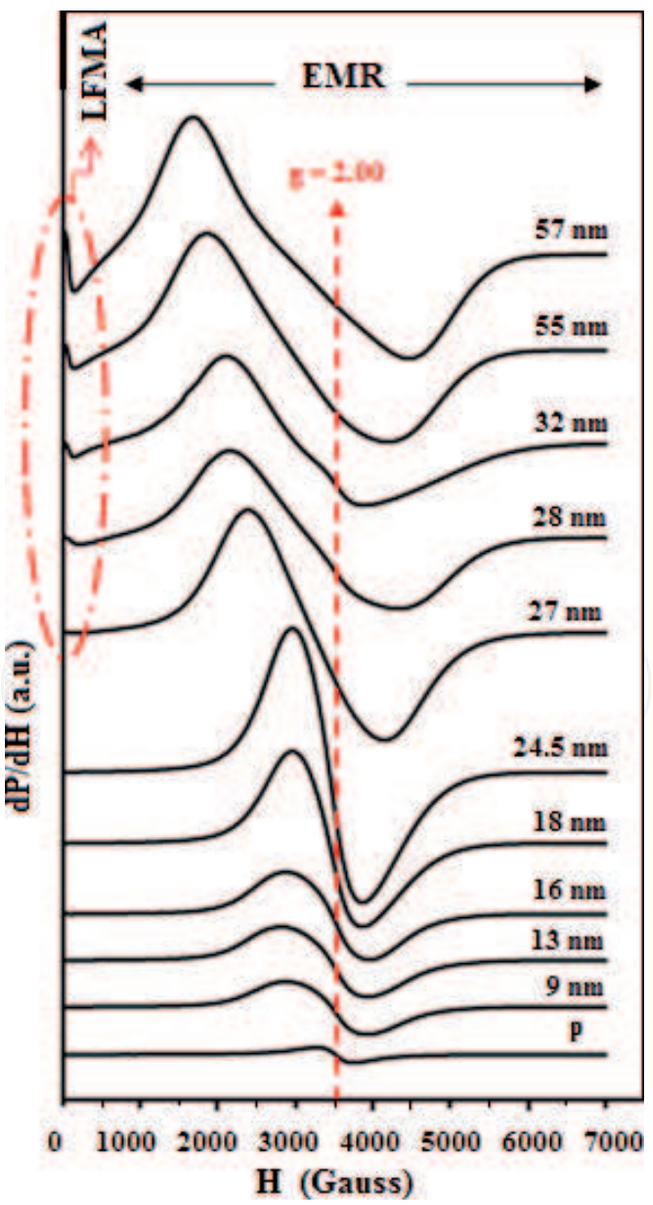

Figure 4.
ESR spectra measured at room temperature for La0.8Sr0.2MnO3 samples with different crystallite sizes [20].

27 nm, the spectra are formed by a single narrow line observed at the higher magnetic field (greater than 1500 G), which can be straightforwardly associated with the electron magnetic resonance absorption (EMR). The EMR is specifically associated with resonant absorption and hence resonant transitions between energy levels by Zeeman effect. This absorption is symmetric with a Lorentzian line shape. Resonance field position stays roughly constant around 3500 G, with g-factor ~ 2 for samples not exceeding 24.5 nm. These spectra are comparable to those of perovskite manganite in a parametric state observed above the Curie temperature. For sizes larger than 27 nm, signal is formed by two absorptions. A strong absorption at high field corresponds to EMR absorption. An additional absorption in the low-field range less than 1000 G is associated with the low-field microwave absorption. As the crystallite size increases, the EMR absorption mode changes toward a broad asymmetric line of Dyson-type and resonance field shifts toward lower values [19, 41].

EMR is a resonant absorption that satisfies Larmor's condition defined by the expression $\omega = \gamma H$, where ω is the resonance frequency, γ is the gyromagnetic factor, and H is the total field on the spins.

In the ferromagnetic samples with spontaneous magnetization resulting from parallel alignment of spins by magnetic interaction effect, the internal fields Hint is added to the applied field giving rise to a total field H = H0 + Hint [42]. The resonance condition is reached at low values of external field to satisfy the Larmor relation [21, 23].

Strontium doping transforms $La_{1-x}Sr_xMnO3$ manganites into a ferromagnetic state at room temperature, due to the reinforcement of the double exchange (DE) interactions between Mn^{3+} and Mn^{4+} ions, which is a ferromagnetic interaction. The ferromagnetic transition depends on the strontium content [43, 44]. The Curie temperature (TC) increases monotonically with x, and TC is increased from 220 to 325 K for values of x between 0 and 0.2 [18, 45].

Zoom of the spectral region from 3100 to 3700 G **Figure 5(a)**) shows that the samples with crystallite sizes below 28 nm have a resonance field (Hres) between 3200 and 3500 G (g-factor between 2.04 and 2.21). These values are lower than the typical value of paramagnetic manganites which is equal to Hres = 3528 G (g = 1.98) [46]. In addition to that, g-factor is bigger than the value of the free electron (ge = 2.0023) [47].

All the samples are attracted by a magnet which confirms the ferromagnetic state. Thus, the presence of the internal field leads to the displacement of the resonance field toward the weak field compared to that of the paramagnetic manganites. On the other hand, the decrease of Hres with decreasing crystallite size is an indication of a reduction in the internal field. Ferromagnetic manganite nanoparticles of few tens of nanometers are formed by a core-shell structure [34]. The core is a ferromagnetic volume enveloped by a magnetically dead layer that contains most of the oxygen defects and the faults in crystallographic structure.

When the particle size is reduced to the nanoscale, two sources contribute to decreasing ferromagnetic volume of manganite. First, the percentage of dead layer increases with increased surface/volume ratio. In addition to that, the shell thickness increases and the volume of the magnetic core decreases [34, 48]. Magnetization of the shell is considered as null, and the contributory portion of each crystallite to the magnetization is the core.

On the other hand, the state of agglomeration in the polycrystalline nanoparticles has an effect on the macroscopic magnetic properties [19]. Considering that the crystallites are in intimate contact, the increase in the shell thickness decreases the magnetic exchange energy between the two cores of neighboring particles, which promotes and improves their separation. In addition, the decrease in the size of the magnetic volume provides another source of new properties. In the nanometric state under the effect of the size reduction, the ferromagnetic material goes from a

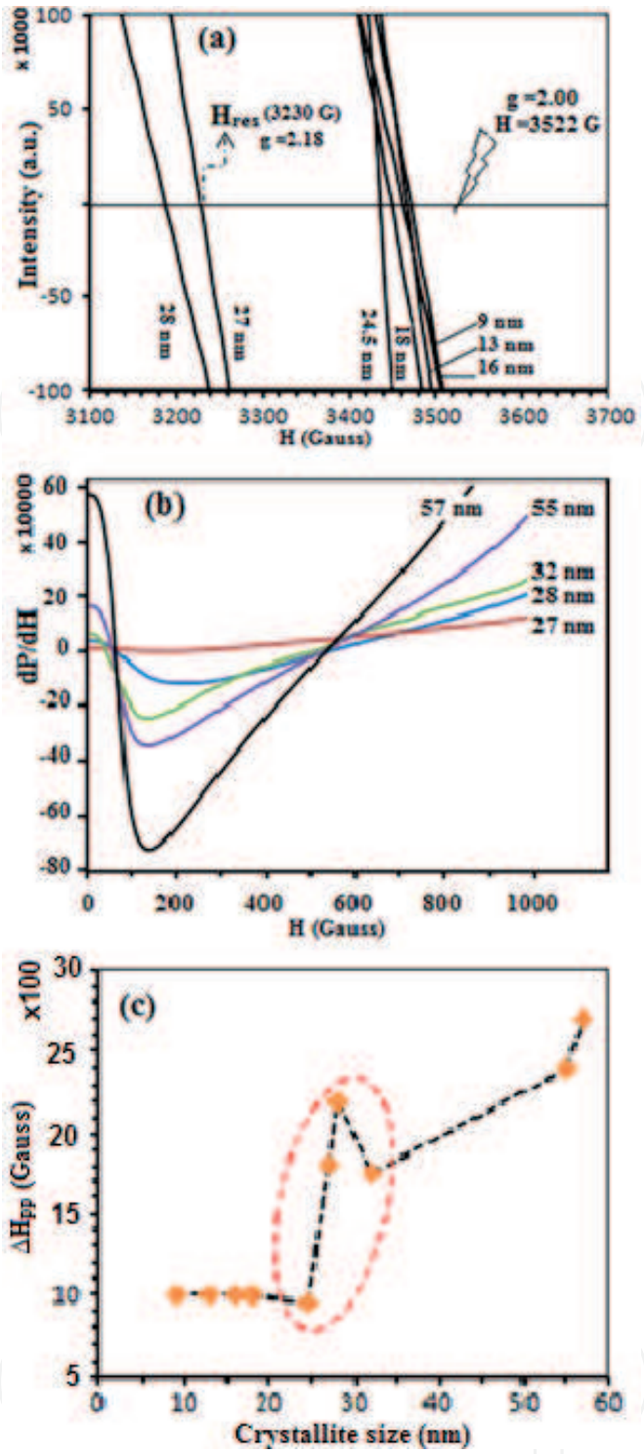

Figure 5.
Variation depending on the crystallite size of: (a) resonance fields in the spectral zone of 3100–3700 G, (b) low field microwave absorption and (c) linewidth ΔHpp [20].

multi-domain state to a magnetic single-domain state and then to the superparamagnetic state. The changes observed in the EMR and LFMA signal appear to be indicative of these magnetic state transitions.

4. Low-field microwave absorption

A zoom on the low-field spectral region (**Figure 5(b)**) shows that the intensity of LFMA gradually decreases with decreasing crystallite size and disappears from 27 nm. This microwave absorption, around zero fields, is a nonresonant absorption.

In ferromagnetic materials, magnetic domains are in a fragile state of equilibrium, and the Bloch wall which is a narrow transition region at the boundary between magnetic domains moves with very low applied fields. In fact, LFMA is associated with dynamics of the magnetic domains in material [49]. The existence of this absorption at room temperature is an indication of the ferromagnetic state of the material used to detect magnetic order. For bulk samples, the LFMA signal is used to determine the Curie temperature of ferromagnetic compounds [23, 50]. Above 28 nm the existence of LFMA shows that these compounds are in a magnetic multi-domain state and a flat response for compounds with smaller size shows that they are in a single-domain state. According to Montiel et al., the absence of LFMA signal in the ferromagnetic compounds is a good indication of superparamagnetic state in the samples [21, 22]. By size reduction, the nanocrystalline passes from a particle with several magnetic domains to a monodomain particle; the latter is either in a single-domain state or in a superparamagnetic state. Low-field absorption cannot determine the intermediate state.

Particles belonging to the single-domain state are characterized by maximum magnetocrystalline anisotropy energy; consequently the direction of magnetization is "frozen.' This characteristic has an effect on the linewidth of resonant absorption; a comparative analysis can reveal the critical size of changes in magnetic states.

5. Electronic magnetic resonance

The peak-to-peak EMR linewidth ΔHpp is an important parameter in measuring magnetic property.

ΔHpp may be due to various factors, namely, magnetic anisotropy field (ΔHK), sample porosity (ΔHpor), demagnetization field (ΔHD), and eddy currents (ΔHeddy) [51]. In the polycrystalline particles, the crystallites are randomly oriented; in that case, the contribution of the magnetocrystalline anisotropy field is dominant and we can have the following approximation Hpp=HK [52].

Linewidth ΔHpp plotted as a function of the crystallite sizes shown in **Figure 5(c)** can be subdivided into three regions. The first part, corresponding to samples with crystallite sizes less than 24.5 nm, ΔHpp has a low value around 1000 G, and between 27 and 32 nm and ΔHpp greatly increases and goes through a maximum at 28 nm. Finally, for sizes greater than 32 nm, ΔHpp increases with a lower slope. This curve calls back the variation of coercivity (Hc) with the particle size, which is maximal for particles in a single-domain state [18].

The magnetocrystalline anisotropy energy in the superparamagnetic state is small and comparable to thermal energy. By random fluctuations of the magnetization due to thermal excitation, the directions of easy magnetization vanish. This is reflected in the low value of ΔHpp [53]. A narrow resonance line is considered as the fingerprint of superparamagnetism at high temperatures, where the energy barrier is dominated by thermal oscillations [54, 55]. Thus, particles smaller than 24.5 nm are in a superparamagnetic state.

Important resonance broadening occurring at superparamagnetic zone boundary indicate that the samples with crystallites size 27, 28, and 32 nm are single-domain ferromagnetic. In the particle formed by a single magnetic domain, the magnetocrystalline anisotropy energy is proportional to the magnetic volume (EB = K V, where K and V are the anisotropy constant and volume of the particle) [56]. In the single-domain region, energy barrier separating two directions of easy magnetization is high. The magnetization requests more energy to get itself aligned along the applied field. The angular dependence of the ΔHpp results in significant increases in linewidth [42].

In the multi-domain state, application in the measurement of weak magnetic field can easily move the magnetic domain walls. The magnetization vectors approach the direction of the applied field, thus leading to reduce ΔHpp. Thus, the decrease of ΔHpp in addition to the appearance of the absorption at low field confirms multi-domain state of samples higher size 32 nm.

These results are comparable to the overall results obtained with samples of analogous compositions [35, 57]. In particular, Sujoy R. et al. reported an exponential increase of the magnetic core between 8 and 22 nm [18], favoring the transition from superparamagnetic state to the single-domain ferromagnetic state.

In addition to the intrinsic causes of line broadening due to the change of magnetic state, extrinsic causes related to the size and shape of the magnetic particles are to be considered. Nanocrystalline powders are formed by several crystallites bonded together to form a wide variety of sizes and shapes that have different magnetic properties [58, 59]. "Crystallite size" is not synonymous with "particle size"; X-ray diffraction is sensitive to the size of crystallite inside the particles.

To study the effect of particle sizes on the line shape, ESR measurements have been performed for two populations with diverse particle size selected by magnetic separation from the sample LSr900- 15 h (55 nm).

6. Effect of particle size

6.1 Magnetic separation of the nanoparticles

The force exerted on a magnetic particle placed in a static magnetic field is proportional to its volume (FM~Vp) [58]. So, according to their sizes, magnetic nanoparticles dispersed in a liquid can be efficiently separated by static magnetic field. In the experiment, the LSr900-15 h powder is dispersed in distilled water with mechanical stirring and then subjected to a magnetic field applied by a permanent magnet. The powder retained after 5 minutes is designated by LSr900b (bigger), and the powder retained from the supernatant after 30 minutes is designated by LSr900s (smaller).

6.2 Structural characterization sand ERS measurement

Figure 6 shows X-ray diffraction patterns of powders LSr900b and LSr900s with LSr900-15 h. The diffraction peaks are characteristic of the perovskite phase. The broadening of the (0 2 4) reflection at $2\theta = 46°$ is in harmony with that of the original compound LSr900-15 h. Thus, the crystallite's size for all the compounds is 55 nm.

The ESR spectra obtained for the three samples have the same general shape (**Figure 7**). They are characteristic of a multi-domain ferromagnetic compound. In coherence with the results of Valenzuela et al., the LFMA signal becomes more intense with increased particle sizes [24]. The linewidth ESR depends on particle sizes, shows a gradual decrease with decreasing size, and is explained by external causes resulting from a distribution of the anisotropy axes [60]. In fact, when a ferromagnetic particle is exposed to a magnetic field, the crystallites tend to orient in the direction of easy magnetization. The assembly of these crystallites in agglomerates prevents some of them from being oriented in the preferred direction, which translates to the spectrum level by the widening of the ESR lines. These observations confirm that the absorption line envelops ensembles of narrower and indistinguishable lines, each of them coming from the resonance of a set of spins called by Portis "spin packets" [61].

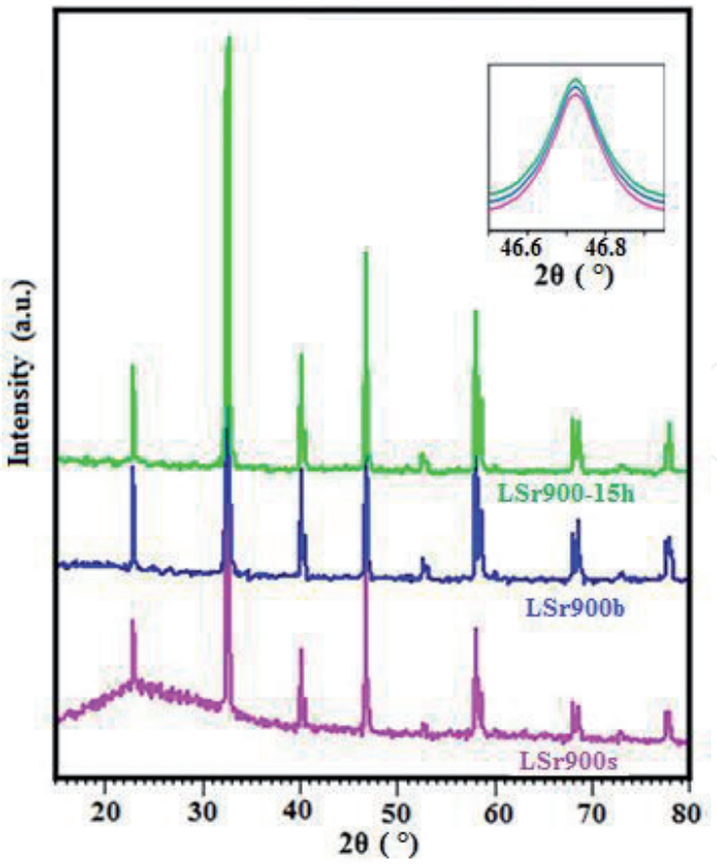

Figure 6.
X-ray diffraction patterns of the samples LSr900-15h, LSr900b and LSr900s. Inset shows the details of the (0 2 4) reflection.

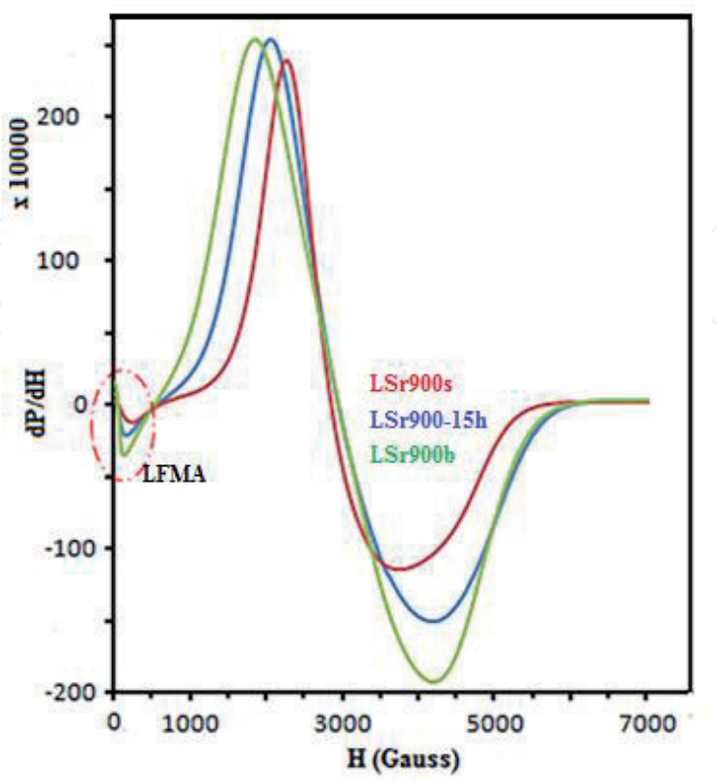

Figure 7.
ESR spectra of the samples LSr900-15h, LSr900a and LSr900b.

However, the resonance frequency remains constant, equal to Hres = 2920 G for the three samples. This can be explained in terms of the same internal field, which is directly related to the crystallite size without exchange interaction between adjacent crystallite. Autocombustion synthesis gives voluminous powders of high specific surfaces, with a structure of "sponge" form [62, 64]. These structures weaken the exchange interactions between the crystallites. In addition to this, the formation of a magnetically dead layer, which increases in thickness with decreasing crystallite size, prevents crystallite-crystallite interactions [34, 62, 63]. Thus, the resonance field is controlled principally by crystallite size.

7. Dependence of the g-factor with the crystallite size

7.1 Detection of magnetic states transitions by g-factor

The Landé g-factor is a dimensionless number calculated from the resonance field based on equation $g = h\nu/\mu BHres$. The curve of g-factor variation as a function of crystallite size can be subdivided into three parts (**Figure 8**). The first is with g values around 2.05, corresponding to the samples with crystallite sizes less than 24.5 nm. This value is slightly higher than that of the typical value of perovskite manganite materials in a paramagnetic state (g = 1.996) [46]. A strong increase in g-factor was observed in the intermediate region corresponding to the samples with crystallite sizes of 24.5 and 32 nm. In the last region, corresponding to the samples with larger crystallite sizes above 32 nm, the g-factor value continues to increase with a lower slope.

The observed slope changes coincide with those reported variations of the linewidth and other ESR spectrum parameters (line shape, LFMA, etc.). So, these changes reflect transitions of magnetic states, from superparamagnetism to ferromagnetism and from single-domain to multi-domain.

To confirm this hypothesis, magnetization measurements were recorded at 300 K and 360 K, collected in a vibrating sample magnetometer (VSM), for the three samples (a) LSr700-2 h (16 nm), (b) LSr700- 24 h (28 nm), and (c) LSr900-15 h (55 nm), belonging to different regions (**Figure 9**).

At room temperature (300 K), the nonlinearity in magnetization curves confirms the ferromagnetic behavior of three samples, while the linearity of the magnetization curve recorded at 360 K reflects a typical paramagnetic character [32]. The magnetization for samples (a) reaches more than 90% of its experimental saturation (Ms) value just above 0.5 T. Moreover, the very small residual magnetization (Mr) considered to be negligible reflects the superparamagnetic character of this sample [64, 65]. The existence of a thick dead magnetic layer in the superparamagnetic state explains the decrease of the saturation magnetization [13, 17].

A magnetization/demagnetization curve of the samples (b, c) with hysteresis loops characterizes the materials in a ferromagnetic state. For sample (b) there is no complete saturation even in the vicinity of 5 T. This means that the magnetic moments are blocked and their alignment toward the applied field requires larger values; this characterizes single-domain ferromagnetic particles [13, 17] Moreover, magnetic remanence (Mr) practically equals 0.5 Ms.; this value is consistent with the model established by Stoner and Wohlfarth for single-domain ferromagnetic particles [66, 67].

Significant reduction in Ms. for the sample (a) compared to samples (b, c) is coherent with both ESR measurements (low factor g) and core-shell model [68]. The core-shell model assumes the formation of a magnetically dead layer of thickness t, which increases with size reduction and can be estimated using the following formula [48]:

$$t = \frac{d}{2}\left(1 - \frac{M_{s\,(nano)}}{M_{s\,(bulk)}}\right)^{1/3} \quad (1)$$

where t is dead layer thickness and d is crystallite size.

As a necessary condition for superparamagnetism, nanoparticles must be formed by small magnetic volumes without exchange interaction [68]. The previous formula shows a significant increase in the dead layer for sizes below 24.5 nm, which has favored superparamagnetism. ESR spectra for these compounds have similarities: narrow linewidth, symmetrical form, g-factor less than 2.08, and absence of LFMA.

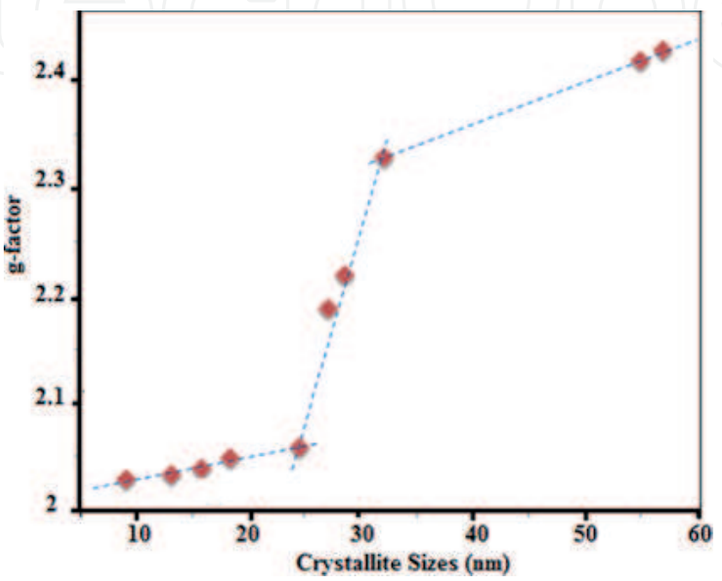

Figure 8.
The change of g-factor with crystallite size.

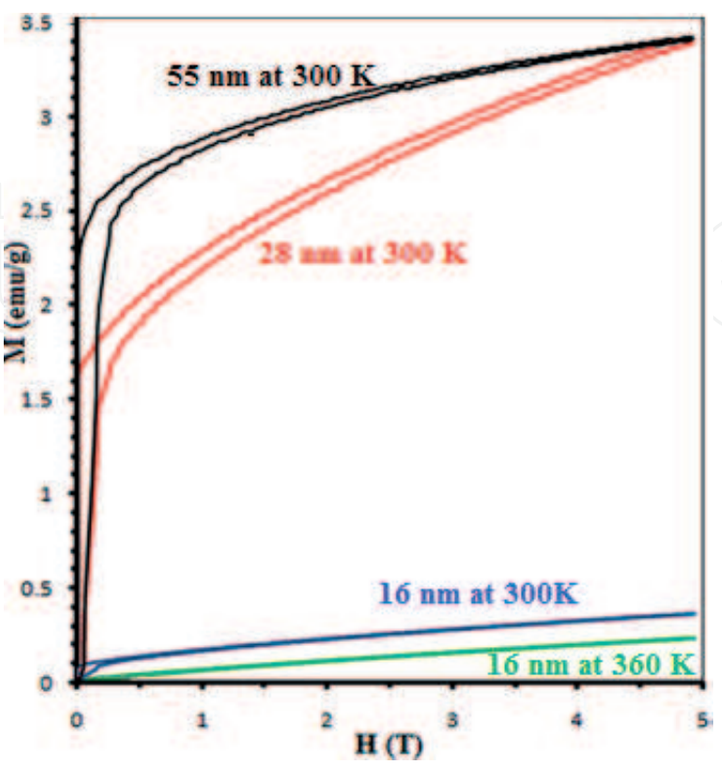

Figure 9.
Magnetization/demagnetization curves of the samples with the crystallite sizes 28 and 55 nm recorded at 300 K. and for sample of 16 nm recorded at 300 K and 360K.

The increase in the magnetic volume due to a sharp decrease in the thickness of the dead layer between 24.5 and 32 nm breaks the superparamagnetism. The system evolves toward the single-domain state, which results in a significant increase of the g-factor and ΔHpp. Beyond 32 nm, nanoparticles change into a multi-domain state. This passage is confirmed by the asymmetrical EMR signal and the appearance of the LFMA.

These results are similar to those of the literature for manganite with the perovskite structure of similar composition [18, 35, 58].

7.2 Superparamagnetic crystallite with multicore

In **Figure 8**, we notice that in the powders with crystallite size less than 24.5 nm (superparamagnetic region), the value of the factor g is practically constant. This suggests that the magnetic core size is invariant regardless of crystallite size.

To rely on the core-shell model with a single magnetic core, in order that the magnetic core keeps the same volume, the thickness of the dead layer must increase with increasing crystallite size. This hypothesis is in contradiction with the literature which reveals that the thickness of the shell decreases [18, 34, 48]. To explain these experimental data, we resorted to the phenomena of magnetic phase separation, which is a usual phenomenon observed in manganites [69, 70]. The competition between several interactions in perovskite manganites means that there are only small energy differences between the different possible phases of the system. As a result, the perovskite manganite oxide is magnetically inhomogeneous, consisting of different spatial regions with different magnetic orders.

Phase separation leads to the formation of a nanometer-sized ferromagnetic droplet cloud ranging from tens of nanometers to several hundred nanometers [71, 72]. In particular, $La_{1-x}Sr_xMnO3$ manganites tend to form mixed phases near the paramagnetic-ferromagnetic phase transition [65, 73]. In this case, transition from the single-domain to the superparamagnetic state is not due to increasing the thickness of the dead layer but to the subdivision of the magnetic volume in small volumes. Thus, the superparamagnetic particles are formed by a paramagnetic volume containing several distinct magnetic cores that we have called superparagmanetic multicore crystallite.

The multicore superparamagnetic state has a comparable magnetic structure with multicore magnetic particles (MCP)that have been shown to be promising for a wide range of biomedical applications, in particular in magnetic hyperthermia treatment and magnetic resonance imaging [74, 75]. So, we can conclude that control of crystallite size in the synthesis of manganites allows a controlled change of magnetism in these compounds.

8. Conclusion

In recent years, a remarkable progress has been made in understanding the magnetic phenomenon in nanomanganites with perovskite structure. This advance is mainly made possible through experimental measurements and theoretical approaches. In this work, ESR spectroscopic measurements were adopted to study crystallite size-dependent magnetic properties of $La_{0.8}Sr_{0.2}MnO_3$ nanomanganite. Samples with different crystallite sizes ranging from 9 to 57 nm were prepared by autocombustion method with a two-step synthesis process. Significant differences in the ESR spectrum parameters, namely, resonant field (Hres), line shape, low-field microwave absorption, and linewidth (ΔHpp), are used to determine the critical sizes of magnetic state changes. The findings from the ESR measurements

are confirmed by VSM measurements. Anomaly observed in the superparamagnetic state has been explained by the formation of multicore magnetic crystallites. These results show the potential use of nanoparticles with crystallite size less than 24.5 nm for biomedical applications. Multicore superparamagnetic state has interesting magnetic properties and can have a large heating capacity equivalent to the magnetic nanoflowers.

Author details

Mondher Yahya[1*], Faouzi Hosni[2] and Ahmed Hichem Hamzaoui[1]

1 Laboratory of Useful Materials Valuation, National Center for Research in Materials Sciences, Soliman, Tunisia

2 Faculty of Sciences, University of Bisha, Bisha, Saudi Arabia

*Address all correspondence to: mondher.yahya@cnrsm.rnrt.tn

References

[1] Hussain BHKI, Anwar MS, Kim JW, Chung KC. Influence of La addition on the structural, magnetic and magnetocaloric properties in Sr2−xLaxFeMoO6 (0x0.3) double perovskite. Ceramics International. 2016;**42**:13098-13103

[2] Lee HS, Park CS, Park HH. Effect of La3+ substitution with Gd3+ on the resistive switching properties of La0.7Sr0.3MnO3 thin films. Applied Physics Letters. 2014;**104**:0-5. DOI: 10.1063/1.4876115

[3] Xu D, Luo L, Ding Y, Xu P. Sensitive electrochemical detection of glucose based on electrospun La0.88Sr0.12MnO3 naonofibers modified electrode. Analytical Biochemistry. 2015;**489**:38-43. DOI: 10.1016/j.ab.2015.08.013

[4] Nandwana V, Ryoo SR, Kanthala S, McMahon KM, Rink JS, Li Y, et al. High-density lipoprotein-like magnetic nanostructures (HDL-MNS): Theranostic agents for cardiovascular disease. Chemistry of Materials. 2017;**29**:2276-2282. DOI: 10.1021/acs.chemmater.6b05357

[5] Mornet S, Vasseur S, Grasset F, Veverka P, Goglio G, Demourgues A, et al. Magnetic nanoparticle design for medical applications. Progress in Solid State Chemistry. 2006;**34**:237-247. DOI: 10.1016/j.progsolidstchem.2005.11.010

[6] Pollert E, Veverka P, Veverka M, Kaman O, Závěta K, Vasseur S, et al. Search of new core materials for magnetic fluid hyperthermia: Preliminary chemical and physical issues. Progress in Solid State Chemistry. 2009;**37**:1-14. DOI: 10.1016/j.progsolidstchem.2009.02.001

[7] Berkova Z, Jirak D, Zacharovova K, Lukes I, Kotkova Z, Kotek J, et al. Gadolinium- and manganite-based contrast agents with fluorescent probes for both magnetic resonance and fluorescence imaging of pancreatic islets: A comparative study. ChemMedChem. 2013;**8**:614-621. DOI: 10.1002/cmdc.201200439

[8] Eguchi A, Mulya A, Lazic M, Radhakrishnan D, Berk MP, Povero D, et al. Microparticles release by adipocytes act as "find-me" signals to promote macrophage migration. PLoS One. 2015;**10**:1-19. DOI: 10.1371/journal.pone.0123110

[9] Sato I, Umemura M, Mitsudo K, Fukumura H, Kim JH, Hoshino Y, et al. Simultaneous hyperthermia-chemotherapy with controlled drug delivery using single-drug nanoparticles. Scientific Reports. 2016;**6**:1-12. DOI: 10.1038/srep24629

[10] Pillai G, Cox A, Yuen L. The science and technology of cancer theranostic nanomedicines: A primer for clinicians and pharmacists. SOJ Pharmacy & Pharmaceutical Sciences. 2018;**5**:1-17. DOI: 10.15226/2374-6866/5/2/00178

[11] Rosensweig RE. Heating magnetic fluid with alternating magnetic field. Journal of Magnetism and Magnetic Materials. 2002;**252**:370-374

[12] Vines JB, Yoon J-H, Ryu N-E, Lim D-J, Park H. Gold nanoparticles for photothermal cancer therapy. Frontiers in Chemistry. 2019;**7**:1-16. DOI: 10.3389/fchem.2019.00167

[13] Leslie-Pelecky DL, Rieke RD. Magnetic properties of nanostructured materials. Chemistry of Materials. 1996;**8**:1770-1783. DOI: 10.1021/cm960077f

[14] Busquets M, Espargaró A, Sabaté R, Estelrich J. Magnetic nanoparticles cross the blood-brain barrier: When physics rises to a challenge. Nanomaterials.

2015;**5**:2231-2248. DOI: 10.3390/nano5042231

[15] Lee JS, Cha JM, Yoon HY, Lee JK, Kim YK. Magnetic multi-granule nanoclusters: A model system that exhibits universal size effect of magnetic coercivity. Scientific Reports. 2015;**5**:1-7. DOI: 10.1038/srep12135

[16] Sharma VK, Waldner F. Superparamagnetic and ferrimagnetic resonance of ultrafine Fe3O4particles in ferrofluids. Journal of Applied Physics. 1977;**48**:4298-4302. DOI: 10.1063/1.323418

[17] Chérif W, Ellouze M, Lehlooh A-F, Mahmood SH, Elhalouani F. Structure, magnetic properties and Mössbauer spectra of La0.67Sr0.33F xMn1-xO3 manganites oxide prepared by mechanical ball milling method. Hyperfine Interactions. 2012;**211**:153-164

[18] Sujoy R, Dubenko I, Edorh DD, Ali N. Size induced variations in structural and magnetic properties of double exchange La0.8Sr0.2MnO3-δ nano-ferromagnet. Journal of Applied Physics. 2004;**96**:1202-1208. DOI: 10.1063/1.1760230

[19] Hintze CE, Fuchs D, Merz M, Amari H, Kübel C, Huang M, et al. Size-induced changes of structural and ferromagnetic properties in La1-x SrxMnO3 nanoparticles. Journal of Applied Physics. 2017;**121**:214303. DOI: 10.1063/1.4984829

[20] Yahya M, Hosni F, M'Nif A, Hamzaoui AH. ESR studies of transition from ferromagnetism to superparamagnetism in nano-ferromagnet La0.8Sr0.2MnO3. Journal of Magnetism and Magnetic Materials. 2018;**466**:341-350. DOI: 10.1016/j.jmmm.2018.04.050

[21] Montiel H, Alvarez G, Conde-gallardo A, Zamorano R. Microwave absorption behavior in Cr2O3 nanopowders. Journal of Alloys and Compounds. 2015;**628**:272-276. DOI: 10.1016/j.jallcom.2014.11.198

[22] Montiel H, Alvarez G, Conde-Gallardo A, Zamorano R. Effect of the particle size on the microwave absorption in the yttrium-iron garnet. Journal of Nano Research. 2014;**28**:73-81. DOI: 10.4028/www.scientific.net/JNanoR.28.73

[23] Alvarez G, Montiel H, Barron JF, Gutierrez MP, Zamorano R. Yafet-Kittel-type magnetic ordering in Ni0.35Zn0.65Fe2O4 ferrite detected by magnetosensitive microwave absorption measurements. Journal of Magnetism and Magnetic Materials. 2010;**322**:348-352. DOI: 10.1016/j.jmmm.2009.09.056

[24] Valenzuela R, Herbst F, Ammar S. Ferromagnetic resonance in Ni-Zn ferrite nanoparticles in different aggregation states. Journal of Magnetism and Magnetic Materials. 2012;**324**:3398-3401. DOI: 10.1016/j.jmmm.2012.02.051

[25] Owens FJ. DC magnetic field dependent microwave absorption in CMR material, La0.7Sr0.3MnO3. Journal of Physics and Chemistry of Solids. 1997;**58**:1311-1314. DOI: 10.1016/S0022-3697(97)00040-1

[26] Owens FJ. Ferromagnetic resonance observation of a phase transition in magnetic field- aligned Fe2O3 nanoparticles. Journal of Magnetism and Magnetic Materials. 2009;**321**:2386-2391. DOI: 10.1016/j.jmmm.2009.02.135

[27] Apostolov A, Apostolova I, Wesselinowa J. Specific absorption rate in Zn-doted ferrites for self-controlled magnetic hyperthermia. European Physical Journal B. 2019;**92**:58

[28] Rashid AU, Ahmed A, Ahmad SN, Shaheen SA, Manzoor S. Study of specific absorption rate of strontium

doped lanthanum manganite nanoparticles for self-controlled hyperthermia applications. Journal of Magnetism and Magnetic Materials. 2013;**347**:39-44. DOI: 10.1016/j.jmmm.2013.07.045

[29] Owens FJ. Ferromagnetic resonance observation of a phase transition in magnetic field- aligned Fe2O3nanoparticles. Journal of Magnetism and Magnetic Materials. 2009;**321**:2386-2391. DOI: 10.1016/j.jmmm.2009.02.135

[30] Channu VSR, Holze R, Walker EH. Nanostructures for Solid Oxide Fuel Cells. New Journal of Glass and Ceramics. 2013;**2013**:29-33. DOI: 10.4236/njgc.2013.31005

[31] Autret-Lambert C, Jirak Z, Gervais M, Poirot N, Gervais F, Raimboux N, et al. Electron spin resonance and neutron diffraction studies of Nd. Physica B: Condensed Matter. 2007;**19**:5222-5229

[32] Curiale J, Sánchez RD, Troiani HE, Leyva AG, Levy P. Room-temperature ferromagnetism in La2/3Sr13MnO3 nanoparticle assembled nanotubes. Applied Physics Letters. 2005;**87**:43113. DOI: 10.1063/1.1999842

[33] Vázquez-vázquez C, Blanco MC, López-quintela MA, Sánchez RD, Rivas J, Oseroff SB. Characterization of La0.67Ca0.33MnO3±δ particles prepared by the sol–gel route. Journal of Materials Chemistry. 1998;**8**:991-1000

[34] Dey P, Nath TK. Effect of grain size modulation on the magneto- and electronic-transport properties of La0.7Ca0.3Mn O3 nanoparticles: The role of spin-polarized tunneling at the enhanced grain surface. Physical Review B: Condensed Matter and Materials Physics. 2006;**73**:1-14. DOI: 10.1103/PhysRevB.73.214425

[35] Dutta A, Gayathri N, Ranganathan R.Effect of particle size on the magnetic and transport properties of La0.875Sr0.125MnO3. Physical Review B. 2003;**68**:54432. DOI: 10.1103/PhysRevB.68.054432

[36] Pollert E, Kaman O, Veverka P, Veverka M, Marysko M, Záveta K, et al. Core-shell La(1-x)Sr(x)MnO3 nanoparticles as colloidal mediators for magnetic fluid hyperthermia. Philosophical Transactions. Series A, Mathematical, Physical, and Engineering Sciences. 2010;**368**:4389-4405. DOI: 10.1098/rsta.2010.0123

[37] Wilson JILAJC. Seherrer after sixty years: A survey and some new results in the determination of crystallite size. Journal of Applied Crystallography. 1978;**11**:102-113

[38] Tang YK, Sui Y, Xu DP, Qian ZN, Su WH. Study of magnetoresistance in nanostructured La2/3Sr 1/3MnO3 powder compacts. Journal of Magnetism and Magnetic Materials. 2006;**299**:260-264. DOI: 10.1016/j.jmmm.2005.04.009

[39] Turky AO, Rashad MM, Hassan AM, Elnaggar EM, Bechelany M. Optical, electrical and magnetic properties of lanthanum strontium manganite La1-xSrx MnO3 synthesized through the citrate combustion method. Physical Chemistry Chemical Physics. 2017;**19**:6878-6886. DOI: 10.1039/c6cp07333f

[40] Phan TL, Thanh TD, Phan MH, Yu SC. Electron spin resonance spectra of La0.7Cd0.3(Mn, Co)O3 Perovskites. IEEE Transactions on Magnetics. 2014;**50**:1-4. DOI:10.1109/TMAG.2013.2273084

[41] Dyson FJ. Electron spin resonance absorption in metals. II. Theory of electron diffusion and the skin effect. Physical Review. 1958;**98**:349-359

[42] Datt G, Kotabage C, Abhyankar AC. Ferromagnetic resonance of NiCoFe2O4 nanoparticles and microwave absorption properties of flexible NiCoFe 2 O 4 –carbon black/poly(vinyl alcohol) composites. Physical Chemistry Chemical Physics. 2017;**19**:20699-20712. DOI: 10.1039/C7CP03953K

[43] Kinoshita T, Furuyabu T, Adachi M. Synthesis of La 0.75Sr0.25MnO3 fine particles for self- controlled magnetic heating hyperthermia by ultrasonic spray pyrolysis. Japanese Journal of Applied Physics. 2014;**53**:70302. DOI: 10.7567/JJAP.53.070302

[44] Moradi J, Ghazi ME, Ehsani MH, Kameli P. Structural and magnetic characterization of La0.8Sr0.2MnO3 nanoparticles prepared via a facile microwave-assisted method. Journal of Solid State Chemistry. 2014;**215**:1-7. DOI: 10.1016/j.jssc.2014.03.011

[45] Khanduri H, Dimri MC, Vasala S, Leinberg S. Magnetic and structural studies of LaMnO 3 thin films prepared by atomic. Journal of Physics D: Applied Physics. 2013;**46**:175003. DOI: 10.1088/0022-3727/46/17/175003

[46] Causa MT, Alejandro G, Zysler R, Prado F, Caneiro A, Tovar M. Jahn-teller effects on the superexchange interactions in LaMnO3. Journal of Magnetism and Magnetic Materials. 1999;**196**:506-508. DOI: 10.1016/S0304-8853(98)00856-7

[47] Taiwo FA. Electron paramagnetic resonance spectroscopic studies of iron and copper proteins. Spectroscopy. 2003;**17**:53-63. DOI: 10.1155/2003/673567

[48] Moradi J, Ghazi ME, Ehsani MH, Kameli P. Structural and magnetic characterization of La0.8Sr0.2MnO3nanoparticles prepared via a facile microwave-assisted method. Journal of Solid State Chemistry. 2014;**215**:1-7. DOI: 10.1016/j.jssc.2014.03.011

[49] Valenzuela R, Alvarez G, Montiel H, Gutiérrez MP, Mata-Zamora ME, Barrón F, et al. Characterization of magnetic materials by low-field microwave absorption techniques. Journal of Magnetism and Magnetic Materials. 2008;**320**:1961-1965. DOI: 10.1016/j.jmmm.2008.02.008

[50] Gavi H, Ngom BD, Beye AC, Strydom AM, Srinivasu VV, Chaker M, et al. Low- field microwave absorption in pulse laser deposited FeSi thin film. Journal of Magnetism and Magnetic Materials. 2012;**324**:1172-1176. DOI: 10.1016/j.jmmm.2011.11.003

[51] Pacewicz A, Krupka J, Salski B, Aleshkevych P, Kopyt P. Rigorous broadband study of the intrinsic ferromagnetic linewidth of monocrystalline garnet spheres. Scientific Reports. 2019;**9**:9434. DOI: 10.1038/s41598-019-45699-7

[52] Srivastava CM, Patni MJ. Ferromagnetic relaxation processes in polycrystalline magnetic insulators. Journal of Magnetic Resonance (1969). 1974;**15**:359-366. DOI: 10.1016/0022-2364(74)90090-0

[53] Byun TY, Byeon SC, Hong KS, Kim CK. Origin of line broadening in Co-substituted NiZnCu ferrites. Journal of Applied Physics. 2000;**87**:6220-6222

[54] Ivanshin VA, Deisenhofer J, Krug von Nidda H-A, Loidl A, Mukhin AA, Balbashov AM, et al. ESR study in lightly doped La1-xSrxMnO3. Physical Review B. 2000;**61**:6213-6219. DOI: 10.1103/PhysRevB.61.6213

[55] Desai P, Song K, Koza J, Pariti A, Nath M. Soft-chemical synthetic route to superparamagnetic FeAs@C core-shell nanoparticles exhibiting high blocking temperature. Chemistry of Materials. 2013;**25**:1510-1518. DOI: 10.1021/cm303632c

[56] Chandra S, Das R, Kalappattil V, Eggers T, Harnagea C, Nechache R, et al. Epitaxial magnetite nanorods with enhanced room temperature magnetic anisotropy. Nanoscale. 2017;**9**: 7858-7867. DOI: 10.1039/c7nr01541k

[57] Krivoruchko VVV, Konstantinova T, Mazur A, Prokhorov A. Magnetic resonances spectroscopy of nanosize La0.7Sr0.3MnO3. Journal of Magnetism and Magnetic Materials. 2006;**300**:e122-e125

[58] Kowalczyk B, Lagzi I, Grzybowski BA. Strategies for size and/or shape-selective purification of nanoparticles. Current Opinion in Colloid & Interface Science. 2011;**16**:135-148. DOI: 10.1016/j.cocis.2011.01.004

[59] Reddy LH, Arias JL, Nicolas J, Couvreur P. Magnetic nanoparticles: Design and characterization, toxicity and biocompatibility, pharmaceutical and biomedical applications. Chemical Reviews. 2012;**112**:5818-5878

[60] Usselman DJSRJ, Russek SE, Klem MT, Allen MA, Douglas T, Young M, et al. Temperature dependence of electron magnetic resonance spectra of iron oxide nanoparticles mineralized in listeria innocua protein cages. Journal of Applied Physics. 2012;**112**:84701

[61] Bowman MK, Hase H, Kevan L. Saturation behavior of inhomogeneously broadened EPR lines detected with magnetic field modulation. Journal of Magnetic Resonance. 1976;**22**:23-32

[62] Yang JYYJ, Wen TL, Tu H, Wang DQ. Characteristics of lanthanum strontium chromite prepared by glycine nitrate process. Solid State Ionics. 2000;**135**:475-479

[63] Zhu T, Shen BG, Sun JR, Zhao HW, Zhan WS. Surface spin-glass behavior in La2/3Sr1/3MnO3 nanoparticles. Applied Physics Letters. 2001;**78**:3863-3865. DOI: 10.1063/1.1379597

[64] Bulte JAFJWM, Brooks RA, Moskowitz BM, Bryant LH. Relaxometry and magnetometry of the MR contrast agent MION-46L. Magnetic Resonance in Medicine. 1999;**42**(2):379-384

[65] Zhang XGLT, Wang XP, Fang QF. Magnetic and charge ordering in nanosized manganites magnetic and charge ordering in nanosized manganites. Applied Physics Reviews. 2014;**1**:31302

[66] Morales AMRMA, Finotelli PV, Coaquira JAH, Rocha-Leão MHM, Diaz-Aguila C, Baggio-Saitovitch EM. In situ synthesis and magnetic studies of iron oxide nanoparticles in calcium-alginate matrix for biomedical applications. Materials Science and Engineering: C. 2008;**28**:253-257

[67] Schrefl JFT, Hrkac G, Suess D, Scholz W. Coercivity and remanence in self-assembled FePt nanoparticle arrays. Journal of Applied Physics. 2003;**93**:7041-7043

[68] Markovich V, Fita I, Wisniewski A, Jung G, Mogilyansky D, Puzniak R, et al. Spin-glass-like properties of La0.8Ca0.2 MnO3 nanoparticles ensembles. Physical Review B: Condensed Matter and Materials Physics. 2010;**81**:134440. DOI: 10.1103/PhysRevB.81.134440

[69] Rivadulla JRF, López-Quintela MA. Origin of the glassy magnetic behavior of the phase segregated state of the perovskites. Physical Review Letters. 2004;**93**:167206

[70] Dagotto AME, Hotta T. Colossal magnetoresistant materials: The key role of phase separation. Physics Reports. 2001;**344**:1-153

[71] Liang L, Li L, Wu H, Zhu X. Research progress on electronic phase

separation in low- dimensional perovskite manganite nanostructures. Nanoscale Research Letters. 2014;**9**:325. DOI: 10.1186/1556-276X-9-325

[72] Saurel CSD, Brûlet A, Heinemann A, Martin C, Mercone S. Magnetic field dependence of the magnetic phase separation in Pr1-xCaxMnO3 manganites studied by small-angle neutron scattering. Physical Review B. 2006;**73**:94438

[73] Ulyanov TEKAN, Yang DS, Mazur AS, Krivoruchko VN, Levchenko GG, Danilenko IA. Local structure and magnetic inhomogeneity of nano-sized La 0.7Sr0.3MnO3 manganites. Journal of Applied Physics. 2011;**109**:0-4

[74] Wells J, Bogart LK, Pankhurst Q, Wells J, Johansson C, Posth O, et al. Standardisation of magnetic nanoparticles in liquid suspension. Journal of Physics D: Applied Physics. 2017;**50**:383003. DOI: 10.1088/1361-6463/aa7fa5

[75] Bender LNP, Bogart LK, Posth O, Szczerba W, Rogers SE, Castro A. Structural and magnetic properties of multi-core nanoparticles analysed using a generalised numerical inversion method. Scientific Reports. 2017;**7**:45990